Classification RNN-Based Equalization for Indoor Non-Line-of-Sight Optical Wireless Communication

Chengwei Fang [1,*], Cuiwei He [2], Estrid He [3], Chen Chen [4], Shuo Li [1], Yinong Wang [5], and Ke Wang [1]
[1]School of Engineering, Royal Melbourne Institute of Technology (RMIT) University, Melbourne, Australia
[2]School of Information Science, Japan Advanced Institute of Science and Technology, Ishikawa, Japan
[3]School of Computing Technologies, Royal Melbourne Institute of Technology (RMIT) University, Melbourne, Australia
[4]School of Microelectronics and Communication Engineering, Chongqing University, Chongqing, China
[5]School of Architecture and Urban Design, Royal Melbourne Institute of Technology (RMIT) University, Melbourne, Australia
[*]Email: chengwei.fang@rmit.edu.au

2025 Asia Communications and Photonics Conference (ACP) | 979-8-3503-5740-0/25/$31.00 ©2025 IEEE | DOI: 10.1109/ACP66871.2025.11350770

***Abstract*—Indoor non-line-of-sight (NLOS) optical wireless communication (OWC) offers robust data transmissions against physical obstacles. This paper proposes an NLOS OWC system with RNN-based classification equalization, and up to 94.8% data rate improvement is experimentally achieved.**

***Keywords*—indoor optical wireless communication, non-line-of-sight, classification recurrent neural network**

I. Introduction

Indoor optical wireless communication (OWC) has emerged as a promising alternative to conventional radio frequency (RF) links, offering high data throughput, low energy consumption, and inherent transmission security [1], [2]. While many indoor OWC systems rely on line-of-sight (LOS) propagation, LOS links in realistic settings are frequently blocked by furniture, occupants, and architectural structures [3]. This motivates non-line-of-sight (NLOS) OWC, where signals arrive via diffusive reflections from walls, ceilings, and furnishings. However, surface absorption and diffusive scattering severely attenuate the received signal, complicating reliable detection. Our previous work demonstrated that practical NLOS links can be enabled using a commercially available silicon photomultiplier (SiPM), which is a high-gain photon-counting detector [4]. In NLOS channels with high-bias SiPM receivers, the maximum achievable rate meeting the hard-decision forward error correction (HD-FEC) threshold (BER = 3.8×10^{-3}) was approximately 80 Mbps, while with low-bias SiPM receivers, the maximum rate meeting the soft-decision forward error correction (SD-FEC) threshold (BER = 2×10^{-2}) was about 100 Mbps [5]. These limits were primarily due to strong multipath-induced inter-symbol interference (ISI), substantial path-loss, and nonlinear detector responses (e.g., SiPMs). These constraints highlight the need for advanced equalization techniques to improve indoor NLOS OWC data rates.

To address these limitations, machine learning-based equalization has emerged as a promising approach for mitigating complex distortions in OWC systems, such as multipath-induced ISI, severe channel attenuation, and nonlinearities of optical components [6]. Among these techniques, recurrent neural networks (RNNs) have proven particularly effective in modeling temporal correlations within received signal sequences, enabling improved compensation for such impairments [7]–[11]. Two main approaches have been explored for applying RNNs in OWC equalization. The first leverages RNNs to process received time-domain signals, aiming to reconstruct the transmitted waveform as accurately as possible before demodulation. For example, [7] proposes a hybrid long short-term memory–deep neural network (LSTM–DNN) channel equalization method for ultraviolet communication systems, achieving average bit error rate (BER) and mean squared error (MSE) reductions of approximately 67.8% and 70.8%, respectively, over traditional methods across signal-to-noise ratio (SNR) from 0 to 20 dB, and demonstrating strong robustness under both low- and high-SNR conditions.

The second approach applies RNNs in a classification framework, where the network directly outputs the most likely transmitted symbol from each received signal segment, rather than reconstructing the entire waveform. This enables the model to learn symbol boundaries and decision regions, which can be particularly effective in reducing BER. For example, [10] proposed an attention-enhanced LSTM-based symbol detection method for a faster-than-Nyquist hybrid modulated OWC system over atmospheric turbulence channels. By training the network to classify received symbols and incorporating an attention mechanism to address the interdependence of adjacent symbols, the proposed method significantly improved BER compared with conventional approaches. Similarly, [11] experimentally demonstrated a bidirectional gated recurrent unit (bi-GRU)-based nonlinear equalizer for high-speed coherent optical communication. In this work, the bi-GRU was trained to classify symbols in the presence of nonlinear distortions, achieving notable performance improvements.

To the best of our knowledge, neural-network-based equalization has not been previously investigated for indoor NLOS OWC links, despite their severe channel impairments and practical relevance. In this paper, we propose a classification RNN-based equalizer employing a bidirectional long short-term memory (Bi-LSTM) architecture to enhance the performance of an NLOS indoor OWC link. Experimental results

show that, under low-bias current conditions (13.5 mA), the proposed method increases the maximum achievable data rate from 100 Mbps to approximately 162.3 Mbps under the SD-FEC threshold, representing a 62.31% improvement over a traditional non-machine-learning-based equalizer. Under high-bias current conditions (21 mA), the data rate increases from 80 Mbps to approximately 159 Mbps under the HD-FEC threshold, corresponding to a 94.8% improvement, and also outperforms a waveform reconstruction RNN equalizer (108 Mbps under HD-FEC). These results demonstrate the potential of the proposed approach in enabling higher-speed and more reliable NLOS OWC links.

II. Classification RNN-based Indoor NLOS OWC System

We first introduce the general concept of an indoor NLOS OWC system, as illustrated in Fig. 1. In such a scenario, an optical transmitter (Tx) emits modulated light signals intended for a receiver (Rx). However, the direct LOS propagation can be obstructed by furniture, occupants, or architectural structures, preventing the Rx from detecting the signal directly. In these cases, the optical signal can still reach the Rx via diffusive reflections from walls, ceilings, and furnishings, enabling NLOS communication.

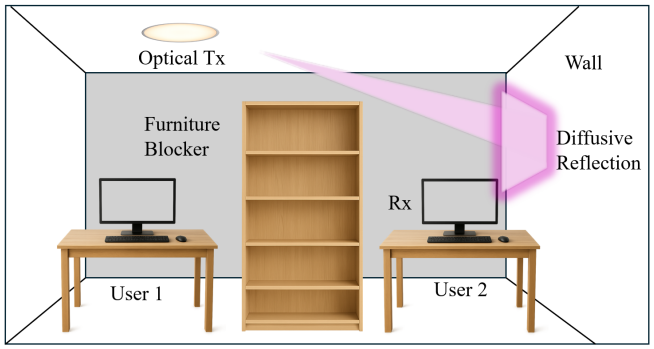

Fig. 1. Indoor NLOS OWC system.

In our setup, we consider 4-ary quadrature amplitude modulation (4-QAM) orthogonal frequency-division multiplexing (OFDM) modulated optical signals, where the receiver output can be modeled as

$$r(t) = s(t) * h(t) + N(t), \tag{1}$$

where $s(t)$ denotes the intensity-modulated optical waveform launched by the transmitter, $h(t)$ is the diffuse indoor channel's impulse response capturing path loss and temporal dispersion due to multiple reflections, and $N(t)$ aggregates additive disturbances from ambient illumination and receiver electronics (shot/thermal noise). The convolution operator $*$ accounts for multipath accumulation along indirect propagation paths.

After timing synchronization, OFDM demodulation is performed to convert the received time-domain sequence into the frequency domain. The discrete-time received sequence $r[n]$ is first segmented into K OFDM symbols, each containing $(N_{\text{cp}}+N)$ samples (including the cyclic prefix). The m-th time-domain symbol vector and the corresponding symbol matrix are given by

$$\mathbf{r}_m^{\text{raw}} = \big[r[m(N_{\text{cp}}+N)], r[m(N_{\text{cp}}+N)+1], \ldots, r[(m+1)(N_{\text{cp}}+N)-1]\big]^\top \in \mathbb{R}^{N_{\text{cp}}+N}, \tag{2}$$

$$\mathbf{R}^{\text{raw}} = \big[\mathbf{r}_0^{\text{raw}}, \mathbf{r}_1^{\text{raw}}, \ldots, \mathbf{r}_{K-1}^{\text{raw}}\big] \in \mathbb{R}^{(N_{\text{cp}}+N)\times K}. \tag{3}$$

Removing the cyclic prefix from each column yields the CP-free symbol matrix

$$\mathbf{R} = \big[\mathbf{r}_0, \mathbf{r}_1, \ldots, \mathbf{r}_{K-1}\big] \in \mathbb{R}^{N\times K}, \tag{4}$$

where $\mathbf{r}_m \in \mathbb{R}^N$ contains only the useful N samples of the m-th OFDM symbol.

Finally, each OFDM symbol $\mathbf{r}_m$ is transformed to the frequency domain via

$$\mathbf{Y}_m = \text{FFT}(\mathbf{r}_m), \tag{5}$$

and collecting all K symbols forms the frequency-domain matrix $\mathbf{Y} \in \mathbb{C}^{N\times K}$.

From the frequency-domain matrix $\mathbf{Y} \in \mathbb{C}^{N\times K}$, only the $K_{\text{eff}} = N/2-1$ data-bearing subcarriers (excluding DC and Nyquist) are retained, with indices $\mathcal{K} = \{1,2,\ldots,K_{\text{eff}}\}$. For the m-th OFDM symbol, the feature matrix is defined as

$$\mathbf{F}_m = \begin{bmatrix} \Re\{Y_m[k]\} \\ \Im\{Y_m[k]\} \\ |Y_m[k]| \\ \angle Y_m[k] \\ \Re\{Y_m[N-k]\} \\ \Im\{Y_m[N-k]\} \\ |Y_m[N-k]| \\ \angle Y_m[N-k] \end{bmatrix}_{k\in\mathcal{K}} \in \mathbb{R}^{8\times K_{\text{eff}}} \tag{6}$$

where each column corresponds to one effective subcarrier, and each row represents one of the eight extracted features: real part, imaginary part, magnitude, and phase for both the subcarrier and its Hermitian-symmetric counterpart. The sequence $\{\mathbf{F}_m\}_{m=0}^{K-1}$ forms the complete input set for the classification RNN.

As illustrated in Fig. 2, the proposed classification RNN-based equalizer comprises an input layer, a Bi-LSTM layer, and a Softmax output layer. The input layer receives $\mathbf{F}_m$ for the m-th OFDM symbol. The Bi-LSTM layer then captures temporal dependencies across consecutive OFDM symbols, exploiting correlations in the frequency-domain symbol sequences. Finally, the Softmax output layer performs multi-class classification independently for each effective subcarrier, producing discrete class labels $\{0,1,2,3\}$ for 4-QAM modulation.

The equalizer output is stored as a $K\times 1$ cell array, where the m-th cell contains the predicted label vector

$$\mathbf{P}_m = [p_m[1], p_m[2], \ldots, p_m[K_{\text{eff}}]] \in \{0,1,2,3\}^{1\times K_{\text{eff}}}, \tag{7}$$

with $p_m[k]$ denoting the detected class label for the k-th effective subcarrier of the m-th symbol. These label vectors

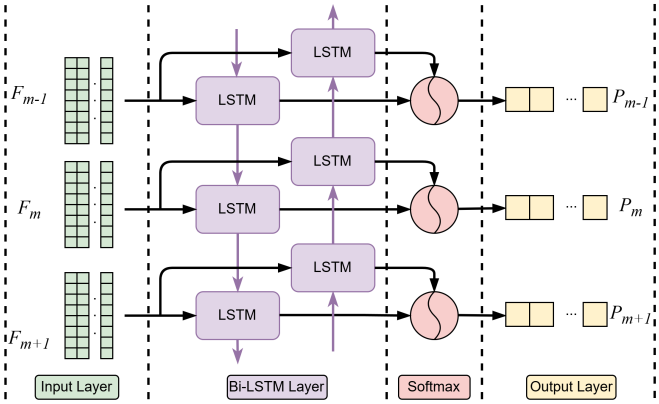

Fig. 2. Structure of classification RNN-based equalizer.

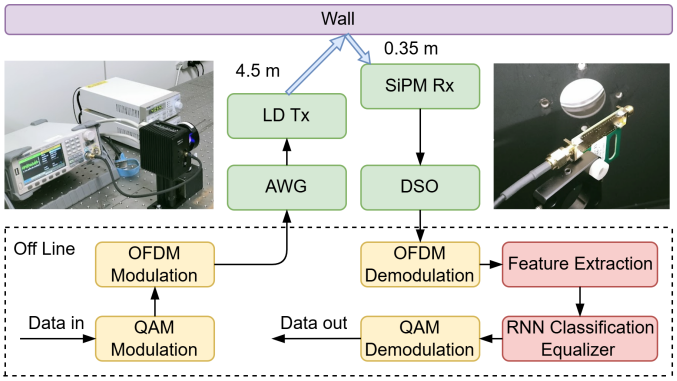

Fig. 3. Experiment of indoor NLOS OWC system with classification RNN-based equalizer.

are passed to the QAM demodulation module, where each label is mapped to its corresponding bit pattern (e.g., 00, 01, 10, 11 for 4-QAM). Concatenating the demodulated bits for all $m = 0, \ldots, K-1$ produces the continuous estimated bitstream at the system output.

It is worth emphasizing that the proposed equalizer is specifically designed and experimentally validated for an indoor NLOS OWC link with a SiPM detector, where direct LOS paths are blocked and signals arrive predominantly via diffuse reflections. Such channels inherently suffer from severe path-loss, multipath-induced ISI, and nonlinear detector responses, which pose significant challenges for reliable high-speed communication. By effectively mitigating these impairments, the proposed RNN-based classification approach not only improves data detection accuracy but also enables the NLOS link to operate at substantially higher data rates under practical indoor conditions.

III. Experiments, Results and Discussion

We first outline the experimental setup of the proposed indoor NLOS OWC system employing a SiPM receiver, as illustrated in Fig. 3. In this configuration, the direct LOS path between transmitter and receiver is intentionally blocked, and the optical carrier reaches the receiver predominantly via diffuse reflections from walls. Binary data are mapped to 4-QAM symbols and modulated using Hermitian-symmetric OFDM, yielding real-valued time-domain waveforms suitable for intensity-modulation/direct-detection (IM/DD). The optical carrier emitted by a laser diode undergoes multiple diffuse reflections before reaching the SiPM. The analog output is digitized by a digital sampling oscilloscope (DSO) and processed offline.

In the experiment, baseband 4-QAM OFDM waveforms are generated in MATLAB and uploaded to an arbitrary waveform generator (AWG; Siglent SDG6052X). The AWG drives a 450 nm laser diode (Thorlabs L450G2) mounted in an LDM56/M with an integrated bias-T. The 450 nm wavelength aligns with the peak photon detection efficiency (PDE) of the SiPM, ensuring high sensitivity. A DC current source (Thorlabs LDC200C) provides the laser bias, while a TEC controller (TED200C) stabilizes the temperature. The beam is directed toward a wall about 4.5 m away, forming a diffuse spot of roughly 30 cm in diameter to realize NLOS transmission.

The scattered light is collected by a SiPM module (ON Semiconductor 30020) mounted on a PCB evaluation board and biased at 28 V. The detector is positioned approximately 0.35 m from the center of the illuminated area to maximize captured diffuse power. Its electrical output, containing both the desired signal and noise from ambient light and receiver electronics, is sampled by a digital sampling oscilloscope (DSO; Rigol DHO4404) for subsequent offline processing.

In the offline processing, we begin by describing the training procedure for the proposed classification RNN equalizer, summarized in Tab. I. The experimental dataset comprises 500 sequences, each containing 256 OFDM symbols modulated with 4-QAM. Each symbol consists of $N = 256$ data samples preceded by a cyclic prefix (CP) of $N_{\text{cp}} = 32$ samples, giving a total length of $(N + N_{\text{cp}}) = 288$ samples per OFDM symbol. Among the subcarriers in each symbol, $K_{\text{eff}} = 127$ are actively used to transmit data. The training set consists of 200 sequences (40%), while the remaining 300 sequences (60%) are reserved for testing and validation.

TABLE I
Training Configuration of the Proposed Classification RNN-based Equalizer.

Hyper-parameter	**Value**
Training sequences	40%
Testing sequences	60%
Input feature size	8
Dropout rate	0.4
Number of classes (M_{QAM})	4
Max epochs	200
Initial learning rate	0.0005
Mini-batch size	32
Loss function	Cross-entropy

For training, each input sample to the network is the feature matrix $\mathbf{F}_m \in \mathbb{R}^{8\times K_{\text{eff}}}$ extracted from the m-th OFDM symbol, where $K_{\text{eff}} = 127$ denotes the number of effective subcarriers. The corresponding target $\mathbf{P}_m \in \{0,1,2,3\}^{1\times K_{\text{eff}}}$ is the ground-truth label vector indicating the transmitted 4-QAM symbol index for each effective subcarrier.

Training is performed using the Adam optimizer with an initial learning rate of 0.0005, reduced every 50 epochs by a factor of 0.75. The loss function is the cross-entropy loss for multi-class classification:

$$\mathcal{L} = -\frac{1}{K_{\text{eff}}} \sum_{k=1}^{K_{\text{eff}}} \sum_{c=0}^{M_{\text{QAM}}-1} \mathbb{1}\{p_m[k] = c\} \log \hat{p}_m^{(c)}[k], \qquad (8)$$

where $\mathbb{1}\{\cdot\}$ is the indicator function, $p_m[k]$ is the true class label for the k-th subcarrier, and $\hat{p}_m^{(c)}[k]$ is the predicted probability of class c output by the Softmax layer.

To evaluate the effectiveness of the proposed classification RNN-based equalizer, we compare its BER performance with that of an RNN-based equalizer that reconstructs the transmitted time-domain signal from the received waveform and a traditional non-machine-learning zero-forcing (ZF) equalizer. All models are tested on the remaining 60% of the dataset (300 OFDM sequences), which are excluded from training. The evaluation covers three target data rates—100 Mbps, 200 Mbps, and 250 Mbps—under four different SiPM bias currents: 10 mA, 13.5 mA, 18 mA, and 21 mA. These bias currents correspond to different incident optical irradiance levels at the SiPM, adjusted via neutral density (ND) filters, with approximate mappings of 13, 20, 35, and 50 mW/m², respectively. The irradiance–current mapping is nonlinear and determined experimentally, as reported in our previous work [5]. For each test configuration, the received signal is processed through the corresponding equalizer, QAM demodulated using standard 4-QAM Gray mapping, and bit-wise reconstructed. The BER is then calculated by comparing the reconstructed bitstream against the original transmitted bit sequence.

The BER performance versus data rate under high SiPM bias currents (18 and 21 mA) is shown in Fig. 4. Across all tested bias currents, the proposed classification RNN enables substantially higher data rates than both the reconstruction RNN and the traditional ZF equalizer, when evaluated under practical FEC thresholds. At 21 mA, for example, the HD-FEC threshold (BER = 3.8×10^{-3}) corresponds to 80 Mbps with ZF equalization and 108 Mbps with the reconstruction RNN, whereas the classification RNN extends this to approximately 159 Mbps—a 94.8% improvement over ZF and a 47.2% improvement over reconstruction RNN. This improvement can be attributed to the classification RNN's ability to directly map noisy frequency-domain features to discrete QAM symbol labels, avoiding the intermediate waveform reconstruction step used in the conventional RNN approach. By bypassing the signal regeneration stage, the proposed method reduces the accumulation of noise and model approximation errors, leading to more reliable symbol detection under challenging high-data-rate conditions.

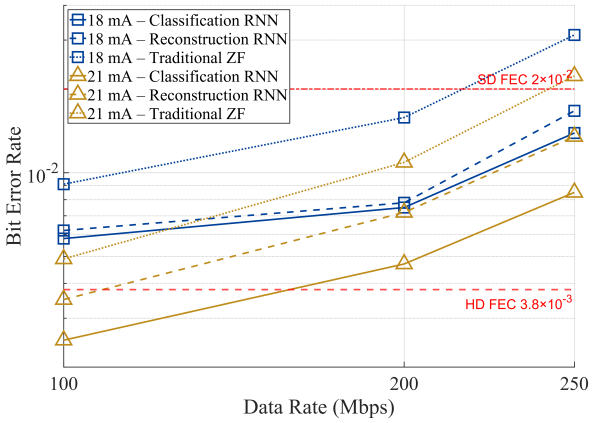

Fig. 4. BER versus data rate under high SiPM bias currents (18 and 21 mA) for classification RNN, reconstruction RNN, and ZF equalizers.

Moreover, we investigate the BER performance versus data rate under low SiPM bias currents (10 and 13.5 mA). The results are shown in Fig. 5. At 13.5 mA, using the SD-FEC threshold (BER = 2×10^{-2}), the proposed classification RNN increases the maximum data rate from 100 Mbps with ZF equalization to approximately 162.3 Mbps—a 62.31% improvement—although this remains slightly below the 171 Mbps achieved by the reconstruction RNN. This slight advantage of the reconstruction RNN may be attributed to its ability to regenerate the continuous waveform before symbol demodulation, which can reduce sensitivity to instantaneous noise in low-data-rate scenarios where ISI is less dominant, whereas the classification approach makes direct symbol decisions that may be more affected by additive noise under such conditions.

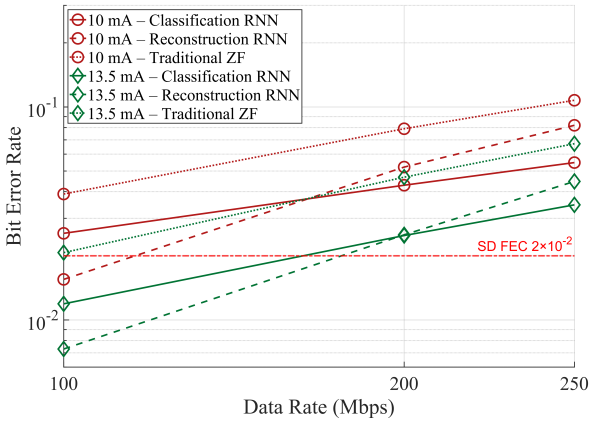

Fig. 5. BER versus data rate under low SiPM bias currents (10 and 13.5 mA) for classification RNN, reconstruction RNN, and ZF equalizers.

IV. Conclusion

In this paper, we proposed a classification RNN-based equalizer for indoor NLOS OWC systems, which directly predicts discrete QAM symbol labels for each effective subcarrier.

The proposed architecture enables efficient end-to-end symbol detection in the presence of severe multipath-induced ISI, path-loss, and receiver nonlinearity. Experimental results show that, the method increases the maximum achievable data rate from 100 Mbps (ZF equalizer) to approximately 162.3 Mbps at 13.5 mA (SD-FEC threshold), and from 80 Mbps (ZF) to approximately 159 Mbps at 21 mA (HD-FEC threshold)—corresponding to 62.31% and 94.8% improvements, respectively. The proposed method enables higher-speed and more reliable indoor NLOS OWC links.

REFERENCES

[1] N. Chi, Y. Zhou, Y. Wei, and F. Hu, "Visible light communication in 6G: Advances, challenges, and prospects," *IEEE Vehicular Technology Magazine*, vol. 15, no. 4, pp. 93–102, 2020.

[2] K. Wang, T. Song, Y. Wang, C. Fang, J. He, A. Nirmalathas, C. Lim, E. Wong, and S. Kandeepan, "Evolution of short-range optical wireless communications," *Journal of Lightwave Technology*, vol. 41, no. 4, pp. 1019–1040, 2023.

[3] K. Wang, A. Nirmalathas, C. Lim, and E. Skafidas, "High-speed optical wireless communication system for indoor applications," *IEEE Photonics Technology Letters*, vol. 23, no. 8, pp. 519–521, 2011.

[4] C. He, Z. Ahmed, and S. Collins, "Signal pre-equalization in a silicon photomultiplier-based optical OFDM system," *IEEE Access*, vol. 9, pp. 23 344–23 356, 2021.

[5] C. He, C. Chen, and K. Wang, "Non-line-of-sight indoor optical wireless communication using a silicon photomultiplier (SiPM)," *Optoelectronics and Communications Conference / International Conference on Photonics in Switching and Computing (OECC/PSC)*, June 2025.

[6] C. Fang, S. Li, Y. Wang, and K. Wang, "High-speed underwater optical wireless communication with advanced signal processing methods survey," *Photonics*, vol. 10, no. 7, p. 811, 2023.

[7] L. Zhang, "Channel equalization in ultraviolet communication based on LSTM-DNN hybrid model," *Scientific Reports*, vol. 15, no. 1, p. 17226, 2025.

[8] J. He, J. Lee, T. Song, H. Li, S. Kandeepan, and K. Wang, "Delay-tolerant indoor optical wireless communication systems based on attention-augmented recurrent neural network," *Journal of Lightwave Technology*, vol. 38, no. 17, pp. 4632–4640, 2020.

[9] J. Lee, T. Song, J. He, S. Kandeepan, and K. Wang, "Recurrent neural network FPGA hardware accelerator for delay-tolerant indoor optical wireless communications," *Optics Express*, vol. 29, no. 16, pp. 26 165–26 182, 2021.

[10] M. Cao, R. Yao, J. Xia, K. Jia, and H. Wang, "LSTM attention neural-network-based signal detection for hybrid modulated Faster-Than-Nyquist optical wireless communications," *Sensors*, vol. 22, no. 22, p. 8992, 2022.

[11] X. Liu, Y. Wang, X. Wang, H. Xu, C. Li, and X. Xin, "Bi-directional gated recurrent unit neural network based nonlinear equalizer for coherent optical communication system," *Optics Express*, vol. 29, no. 4, pp. 5923–5933, 2021.